

# Rocking response of self-centring wall with viscous dampers under pulse-type excitations

Lingxin Zhang<sup>1</sup> Xiaogang Huang<sup>2\*</sup> and Zhen Zhou<sup>2</sup>

<sup>1</sup>Institute of Engineering Mechanics, China Earthquake Administration; Key Laboratory of Earthquake Engineering and Engineering and Engineering Vibration, China Earthquake Administration

<sup>2</sup>Key Laboratory of Concrete and Prestressed Concrete Structures of the Ministry of Education, Southeast University

(Received March 25, 2020, Revised May 20, 2020, Accepted June, 10, 2020)

**Abstract.** A self-centering wall (SCW) is a lateral resistant rocking system that incorporates posttensioned (PT) tendons to provide a self-centering capacity along with dampers to dissipate energy. This paper investigates the rocking responses of a SCW with base viscous dampers under a sinusoidal-type pulse considering yielding and fracture behaviour of the PT tendon. The differences in the overturning acceleration caused by different initial forces in the PT tendon are computed by the theoretical method. The exact analytical solution to the linear approximate equation of motion is also provided for slender SCWs. Finally, the effects of the ductile behaviour of PT tendons on the rocking response of a SCW are analysed. The results demonstrate that SCWs exhibit two overturning modes under pulse excitation. The overturning region with Mode 1 in the PT force cases separates the safe region of the wall into two parts: region S1 with an elastic tendon and region S2 with a fractured tendon. The minimum overturning acceleration of a SCW with an elastic-brittle tendon becomes insensitive to excitation frequency as the PT force increases. After the plastic behaviour of the PT tendon is considered, the minimum overturning acceleration of a SCW is increased significantly in the whole range of the studied  $w_g/p$ .

**Keywords:** self-centering wall; overturning acceleration spectrum; pulse type excitation; viscous dampers; inelastic tendon; analysis and computation

## 1. Introduction

A cast-in-place reinforced concrete wall is a traditional lateral load resisting system widely used in seismic regions, which usually sustains permanent damage caused by yielding and local cracking during earthquakes (Eom et al 2014, Lim and Hong 2014). High post-earthquake repair costs have motivated researchers to investigate self-centering rocking walls (SCWs). The wall is post-tensioned to the foundation with unbonded multi-strand steel tendons. The replaceable or repairable dissipators are introduced into the joint between the walls and the foundation to provide energy dissipation capacity. The new system has exhibited positive effects in the seismic resistance within the design displacement (Xu et al. 2018, Feng et al. 2018). When loaded dynamically, the wall will rock about the foundation and therefore withstands strong earthquake shaking through gap opening mechanisms at the base. The seismic behaviour of SCWs can be approximated as the rocking motion of a rigid block. Rocking motion combines the benefits of rocking isolation with the advantage of the precast method, making the rocking wall have better construction quality and larger drifts with minor damage. Rocking does, however, face a higher risk of an overturning collapse. Posttensioned (PT) tendon and additional dampers will

offer an anchor effect for the rocking response.

Early studies on the rocking response of a rigid block were presented by Housner (1963). Following these studies, the overturning of a rocking block under pulse-type motions has been studied (Makris and Roussos 2000, Zhang and Makris 2001, Makris and Zhang 2001). Near-fault ground motions are pulse-type motions characterized by the period and amplitude of the velocity pulse (Mavroeidis and Papageorgiou 2003, Bray and Rodriguez 2004), which can force the blocks to rock drastically. Recently, the dynamic behaviours of massive structural members such as bridge piers have been analysed under near-fault ground motions. Makris and Vassiliou (2014, 2015) analyzed the dynamics of bridge piers vertically restrained with an elastic tendon through the pier centreline. Giouvanidis and Dimitrakopoulos (2015, 2017) established dimensionless design parameters for the rocking frames comprised of two bridge piers and a heavy cap-beam and examined the seismic behaviour of the bridge system under both pulse-type and historic ground motions.

The significant differences between SCWs and bridge piers in the bending moment capacity, seismic demand and geometric dimensions (Kurama *et al.* 2002, Restrepo and Rahman 2007, Perez *et al.* 2004, 2007, 2013) have driven this paper to theoretically investigate the rocking behaviours of SCWs. The viscous dampers are velocity-dependent energy dissipation systems, which are particularly incorporated to counteract near-fault earthquakes. The full recentering property of a SCW mainly depends on the prestressed tendon. Accordingly, the lateral

\*Corresponding author, Ph.D.

E-mail: [xiaogang\\_huang@hotmail.com](mailto:xiaogang_huang@hotmail.com)

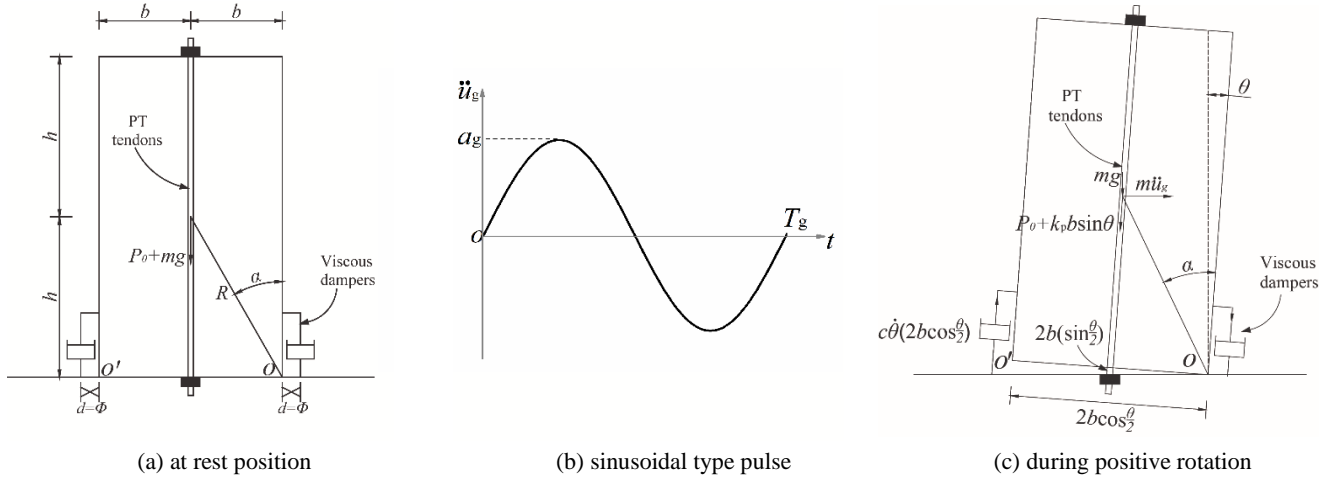


Fig. 1 Schematic diagram of examined rocking wall

stiffness of the system will remain positive upon uplifting due to the large ratio of the elasticity of the tendon to the weight of the wall. The inelastic behaviour of a PT tendon can cause dynamic amplification and even toppling of a SCW (Bruce and Eatherton 2016). It is necessary to investigate whether SCWs will topple under pulse-type excitation considering the inelastic behaviour of the tendon. The overturning acceleration spectrum of SCW is given under one-sine pulse. Both the linear and nonlinear formations for the SCW are derived to facilitate the rocking analysis of SCW. Finally, the effect of the ductile behaviour of the PT tendon on the rocking response of the SCW is analysed.

## 2 Description of self-centering wall

A self-centering wall (SCW) is capable of both surviving significant seismic energy and exhibiting recentering behaviour. The existence of the prestressed tendon can not only provide recentering capacity for the wall but also ensure the positive stiffness of the wall upon uplifting. Tendon yielding or fracture may occur during strong earthquakes due to an increase in substantial tension force from gap opening. The overturning of the wall can be triggered by the initiation of the limit state. The motivation of this study is to analyze the dynamic of the wall with viscous damper. The yielding and fracture of the tendon is considered from the theoretical point. The conclusions will shed some light on the behaviour, performance, and design methodology of the wall under near-fault ground motions.

To investigate the rocking and overturning of a SCW with a central posttensioned (PT) tendon shown in Fig. 1(a), consider an SCW with mass  $m$ , diagonal distance  $R^2 = \sqrt{b^2 + h^2}$  and aspect ratio  $b/h = \tan \alpha$  having base viscous dampers on the edge of the wall subjected to a sinusoidal type ground acceleration  $\ddot{u}_g$  in Fig. 1(b). It is assumed the wall and the base are rigid and the relative sliding motion is entirely avoided. When the imminent uplifting resistance of the SCW is exceeded with increasing acceleration, the SCW will be set into rocking motion about

the pivoting point  $O$  or  $O'$  repeatedly, as shown in Fig. 1(c), where  $\theta$  is the rotation angle of the wall.

Near-fault ground motions containing strong velocity pulses can impose extreme demands on structures and force the SCW to rock drastically. The pulse-type effects can be quantified by equivalent pulses, which replicate comparable near-fault response characteristics using simple parameters (Alavi and Krawinkler 2004). Trigonometric pulses have been selected to illustrate the dynamic responses of a rocking block under near-source ground motion in previous studies (e.g. Zhang and Makris 2001). In this paper, a full-cycle sinusoidal type pulse with acceleration amplitude  $a_g$  and frequency  $\omega_g$  is used to resemble a seismic excitation and its form is shown as follows

$$\begin{cases} \ddot{u}(g) = a_g \sin(\omega_g t + \varphi) & t \leq T_g \\ \ddot{u}(g) = 0 & t > T_g \end{cases} \quad (1)$$

where  $T_g = (2\pi - \varphi) / \omega_g$  is the time instant when the excitation expires and free rocking initiates, and  $\varphi = \arcsin(bg/a_g h + P_0 b/a_g m h)$  is the phase angle when rocking initiates, which is given by the following formula.

The damper force and velocity relation for typical viscous dampers are usually expressed as a fractional velocity power law

$$F_v = c |v|^n \operatorname{sgn}(v) \quad (2)$$

where  $c$  is the damping coefficient, representing the damper force per the damper velocity  $v$  raised to the power of  $n$ ;  $n$  is a positive exponent in the range of 0.1-1 for the seismic application; and  $\operatorname{sgn}$  is the signum function. The viscous dampers undertaken in this study have a coefficient  $c = 10000$  N·s/m and a velocity exponent  $n = 1$ . The function using  $n = 1$  represents a linear viscous damper in which the damper force is proportional to the relative velocity. This linearization also facilitates the derivation of the linear analytical solution in the following section.

Under the negative ground acceleration  $\ddot{u}_g$ , the wall will initially pivot about point  $O$ . It will recenter and pivot about the other point  $O'$  if the toppling of the wall is

avoided. During rocking motion of the wall, in addition to the work of the external forces, work is also done by the axial force in the tendon  $P$  and the damper  $F_v$ . By considering dynamic moment equilibrium, the equations of motion are respectively derived as follows

$$\begin{cases} I_o \ddot{\theta} + mg \cdot R \sin(\alpha - \theta) + c \dot{\theta} (2b \cos \frac{\theta}{2})^2 + P_0 (b \cos \frac{\theta}{2}) + k_p (b \sin \theta) b = -m \ddot{u}_g R \cos(\alpha - \theta) & \theta > 0 \\ I_o \ddot{\theta} + mg \cdot R \sin(-\alpha - \theta) + c \dot{\theta} (2b \cos \frac{\theta}{2})^2 - P_0 (b \cos \frac{\theta}{2}) + k_p (b \sin \theta) b = -m \ddot{u}_g R \cos(-\alpha - \theta) & \theta < 0 \end{cases} \quad (3)$$

where  $\theta$  is the rocking rotation of the wall at arbitrary time instant,  $P_0$  and  $k_p$  are the initial force and stiffness of the PT tendon, respectively, and  $c$  is the damping coefficient of the damper. Following decompression, the tendon elongates  $2b \sin(\theta/2)$ , as shown in Fig. 1(c), producing an increase in its axial force, which eventually becomes  $P_0 + 2k_p b \sin(\theta/2)$ . Moreover, the moment due to the presence of the damper is the product of the total tendon force  $P$  and the moment arm  $b \cos(\theta/2)$ . The moment arm from the damper force is  $2b \cos(\theta/2)$  and therefore the pertinent moment is  $2b F_v \cos(\theta/2)$ . For the rectangular block, the moment of inertia about the pivot point is  $I_o = 4mR^2/3$ . Upon uplifting, static moment equilibrium of the wall about the pivoting point gives  $m \ddot{u}_g h > mgb + P_0 b$ . This means the seismic demand has reached the limit of the seismic resistance. Therefore, the wall will rock when the ground acceleration satisfies  $\ddot{u}_g > bg/h + P_0 b/mh$ . Eq. (3) can also be expressed in a compact form using the signum function

$$\underbrace{I_o \ddot{\theta} + mgR \sin[\alpha \cdot \text{sgn}(\theta) - \theta]}_{\text{rocking wall}} + \underbrace{c \dot{\theta} (2b \cos \frac{\theta}{2})^2}_{\text{damper}} + \underbrace{P_0 (b \cos \frac{\theta}{2}) \cdot \text{sgn}(\theta) + k_p b^2 \sin(\theta)}_{\text{tendon}} = \underbrace{-m \ddot{u}_g R \cos[\alpha \cdot \text{sgn}(\theta) - \theta]}_{\text{seismic excitation}} \quad (4)$$

The contribution of each component in the SCW is described in the above equation. Therefore, the equation can be further simplified as

$$\ddot{\theta} = - \left\{ p^2 \sin[\alpha \cdot \text{sgn}(\theta) - \theta] + \frac{6(b \cos \frac{\theta}{2})^2}{R^2} \zeta p \dot{\theta} + \frac{P_0 b \cos \frac{\theta}{2}}{I_o} \cdot \text{sgn}(\theta) + \frac{k_p b^2}{I_o} \sin(\theta) + \frac{\ddot{u}_g}{g} p^2 \cos[\alpha \cdot \text{sgn}(\theta) - \theta] \right\} \quad (5)$$

where  $p = \sqrt{mgR/I_o} = \sqrt{3g/4R}$  is a measure of the frequency characteristics of the wall, and the larger the wall ( $R$ ), the smaller the  $p$ .  $\zeta = c/2mp$  denotes the damping ratio, which is a dimensionless parameter that relates the damping coefficient  $c$  to the mass  $m$  and frequency  $p$ . Seismic energy dissipation due to each impact at the pivot point  $O$  or  $O^*$  is approximated with a restitution coefficient  $r$ , which is defined as the reduction of the angular velocity

$$\dot{\theta}^+ = \sqrt{r} \dot{\theta}^- \quad (6)$$

where  $\dot{\theta}^+$  is the angular velocity just after impact,  $\dot{\theta}^-$  is the angular velocity just before impact, and  $r$  denotes the restitution coefficient given by

$$r = [1 - \frac{3}{2} \sin^2 \alpha]^2 \quad (7)$$

Although the above derivation of the coefficient  $r$  is derived based on some assumptions (ElGawady *et al.* 2011), Eq. (7) is a widely used method to measure the reduction in

the kinetic energy of the block during the impact. When the angle of rotation  $\theta$  reverses, the product of the angle of rotation  $\theta$  in two adjacent steps is negative. If this condition is satisfied during rocking, the angular velocity in the current step is the restitution coefficient times the angular velocity in the previous step.

### 3. Nonlinear numerical solution

The nonlinear solution of Eq. (4) can be computed numerically by the state-space formulation. The PT tendons are assumed to be elastic until they reach their ultimate strength. If the tendon reaches its fracture elongation  $\mu_s = (F_u - P_0)/k_p$ , the tendon snaps and the rocking rotation  $\theta_s$  at this moment is expressed as

$$\begin{aligned} \theta_s &= 2 \arcsin\left(\frac{\mu_s}{2b}\right) \\ \mu_s &= \frac{F_u - P_0}{k_p} \end{aligned} \quad (8)$$

where  $\mu_s$  is the deformation causing the tendon to snap during rocking.  $F_u$  and  $P_0$  are the ultimate force and initial force of the PT tendon, respectively. The PT tendon is maintained in an elastic status with  $|\theta| \leq \theta_y$ . Once snapping of the PT tendon occurs with  $|\theta| > \theta_y$ , the dynamic equation switches irreversibly to the equation of the free-standing wall

$$\ddot{\theta} = - \left\{ p^2 \sin[\alpha \cdot \text{sgn}(\theta) - \theta] + \frac{6b^2}{R^2} \zeta p \dot{\theta} + \frac{\ddot{u}_g}{g} p^2 \cos[\alpha \cdot \text{sgn}(\theta) - \theta] \right\} \quad (9)$$

By replacing  $\zeta$  with  $\gamma = 3b^2 \zeta / R^2 = 3\zeta \sin^2(\alpha)$ , Eq. (9) is similar to the analytical equation derived by Dimitrakopoulos and DeJong (2012).

A state-space formulation is developed for the wall subjected to the seismic excitation as described in Eq. (1)

$$\{y(t)\} = \begin{Bmatrix} \theta(t) \\ \dot{\theta}(t) \end{Bmatrix} \quad (10)$$

The numerical integration of Eq. (10) is performed by ODE (Ordinary Differential Equation) solvers available in MATLAB. Fig. 2 provides an illustration of three possible normalized rotation histories of the SCW ( $P_0/W = 0$ ): No overturning occurs when the ground acceleration amplitude  $a_g$  is sufficiently small, as shown in Fig. 2(a); the wall continues rocking and will not stop until the mechanical energy is dissipated. Figs. 2(b) and 2(c) show two different modes in which a SCW may topple. With a specific pulse frequency and acceleration excitation, a SCW may overturn with one impact (Mode 1) or overturn directly (Mode 2). The transition from overturning with one impact (Mode 1) to overturning without impact (Mode 2) is not immediate when the excitation acceleration increases. This phenomenon is consistent with previous studies and has been explained by Makris and Zhang (2001). A sensitivity study has been performed to determine the suitable integration step for the calculation of the wall responses. Two integration steps ( $t = 0.0001$  s and  $t = 0.00001$  s) are

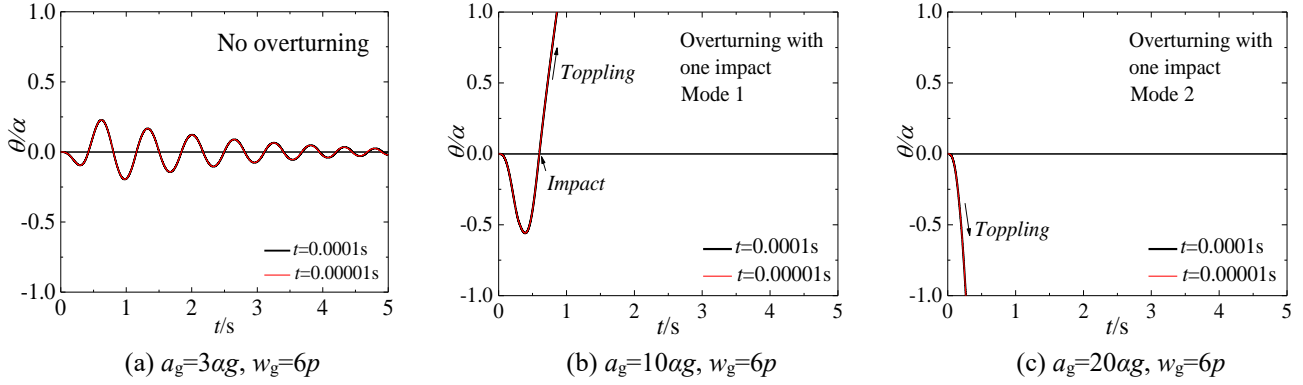


Fig. 2 Mode of a SCW: (a) no overturning (b) Mode 1: overturning with one impact (c) Mode 2: overturning without impact

respectively examined for the computational model. It can be seen that, regardless of the integration step, the two models produce the same results for all of the rocking states. An integration step of 0.0001 s is currently used to obtain accurate numerical solutions and to reduce the computational time.

It is instructive to plot the rocking responses of a SCW by the minimum overturning acceleration spectrum. The overturning acceleration spectrum is a graphical presentation of the relationship in Eq. (3). The concept of the spectrum is introduced to present graphically the pulse amplitude  $a_g$  required to overturn the wall as a function of the pulse frequency  $w_g$ . Both axes are dimensionless, the vertical axis is normalized by the product of the wall slenderness  $\alpha$  and the acceleration of gravity  $g$ , while the horizontal axis by the frequency parameter  $p$ . The boundary lines between the overturning region and the safe region of the wall are plotted in the spectrum. Acceleration amplitudes with magnitudes larger than the bottom line (that corresponds to the minimum overturning acceleration) will be able to overturn the wall.

For illustrative purposes only, the results here are presented in terms of an example. Traditional concrete walls with low height-to-width ratios ( $h/b$ ) produce less energy dissipation due to the highly pinched hysteresis curves (Palermo *et al.* 2002; Sritharan *et al.* 2014). Following the physical characteristics of typical walls, this paper examines a slender rigid wall ( $h/b=5$ ,  $W=25\text{kN}$ ) with frequency parameter  $p=1.70$ , and slenderness  $\alpha=11.31^\circ$ . More details about the effects of the wall slenderness can be found in Apostolou *et al.* (2007). The overturning acceleration spectrum of the corresponding free-standing walls considering the energy loss during each impact ( $\eta = \sqrt{r_{\max}} = 0.95$ ) under a sinusoidal type pulse is plotted in Fig. 3(a). The results are calculated with a state-space formulation given by Eq. (10). It shows that the free-standing wall has two overturning modes. For a small  $\omega_g/p < 4.5$ , the free-standing wall will first topple with Mode 1 as the pulse acceleration increases and then topple with Mode 2 when the SCW suffers higher pulse acceleration. There is a finite margin area of acceleration amplitudes between Mode 1 and Mode 2 in which the free-standing wall remains safe. For values within  $4.5 < \omega_g/p < 10$ ,

overturning with Mode 1 will not happen. The minimum overturning acceleration with Mode 2 is increased sharply as a result of increasing  $\omega_g/p$ . For values of  $\omega_g/p > 10$ , the high frequency exceeds the studied frequency range because the near-source ground motions have attributes of low frequency and large displacement amplitude. Therefore, this paper does not consider the possibility of the combination of two safe regions in the PT force cases after the value  $\omega_g/p$  exceeds 10.

On the basis of the free-standing wall shown in Fig. 3(a), a PT tendon ( $k_p=5.6 \times 10^6 \text{N/m}$ ,  $F_u=7.5W$ ;  $W$  denotes the self-weight of SCW) and a pair of viscous dampers are implemented therein. The tendon has a diameter of 15.3 mm, an area of  $144 \text{mm}^2$ , and a nominal ultimate stress of 1860 Mpa. An elastic-brittle behaviour is assumed for the tendon. The damping coefficient  $\zeta$  of viscous dampers is set to 1.15. Figs. 3(b)-(d) compare the overturning acceleration spectrum of SCW with different PT force cases under a sinusoidal type pulse. Note that the  $P_0/W=0$  case and the free-standing case are not equivalent owing to the existence of elastic coefficient  $k_p$ . Sufficient pretension in the tendon usually causes a larger ratio of  $P_0/W$  and may subsequently affect the rocking responses of the damped SCW. The results are computed for the cases where  $P_0/W=0$ ,  $P_0/W=3$ , and  $P_0/W=6$  using Eq. (10). The results show that SCWs also have two different overturning modes even with different initial forces. However, it is obvious that higher acceleration is needed to topple SCWs in response to a low-frequency pulse after the implementation of a PT tendon and viscous dampers. Taking an example of a given value  $\omega_g/p=2$ , the minimum overturning acceleration of the wall is increased from  $1.3ag$  for the free-standing case to  $7.3ag$  for the  $P_0/W=0$  case,  $7.9ag$  for the  $P_0/W=3$  case and  $9.8ag$  for the  $P_0/W=6$  case. It can be inferred that the existence of the tendon rather than the magnitude of the PT force plays a more important role in increasing the overturning resistance of the SCW in the low  $\omega_g/p$  range. As the value of  $\omega_g/p$  increases, it is more difficult to overturn the free-standing wall due to the disappearance of overturning with Mode 1. The lower bound of the overturning region with Mode 2 in the PT force cases is larger than that of the free-standing wall. However, the overturning area of Mode 1 in the PT force cases separates the safe region into two parts: region S1 with the elastic tendon and region S2 with the fractured

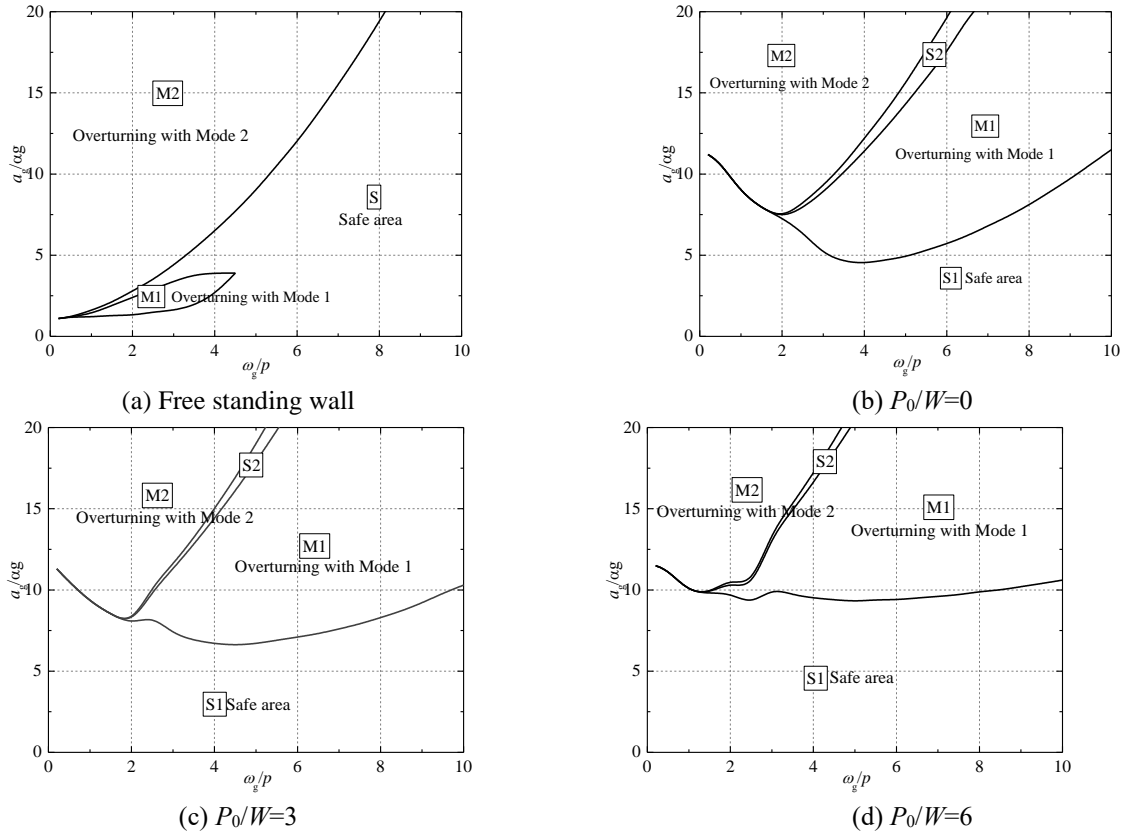


Fig. 3 Overturning acceleration spectrum of a free-standing wall under a sinusoidal type pulse

tendon.

Figs. 3(b) - 3(d) illustrates a similar overturning process for all of the walls with different PT forces in the tendon. When the pulse acceleration is relatively low, the rocking responses of the SCW remain in the safe region S1. Then, the SCW overturns after experiencing one impact (Mode 1) when the minimum overturning acceleration is exceeded. The PT tendon will be fractured under the influence of Mode 1. As the excitation acceleration increases, there is a safe region between the two modes with magnitudes larger than the overturning acceleration corresponding to Mode 1, meaning that it remains standing when the acceleration increases. This is because a SCW with a fractured PT tendon can return back to its initial position induced by the intense acceleration pulse. For even higher levels of acceleration, overturning of the SCW occurs again without impact (Mode 2) after PT tendon rupture directly in response to the oscillation of the wall. Different initial forces  $P_0$  in the PT tendon induce similar rocking trends of SCWs.

The moment associated with the initial forces  $P_0$  in the equation of motion for the rocking mechanism of SCW is becoming dominant compared to the moment associated with gravity force as the  $P_0/W$  increases to 6. The dominant contribution of the strands to the overall behaviours makes the wall insensitive to the excitation frequency. It can be observed in Fig. 3(d) that the minimum overturning acceleration boundary associated with Mode 1 of overturning tends to be a horizontal line as the  $P_0/W$  increases.

The other observation related to varying initial forces  $P_0$  is the overturning acceleration for the prestressed wall is smaller than that of a free-standing wall for a large  $w_g/p$  ratio. Although the increasing forces  $P_0$  in the strands provides an enhanced self-centering capacity for the rocking wall, the fracture of the tendon can cause a significant loss of the tendon contribution and trigger an entirely different kinematic mechanism in the wall. Makris and Zhang (2001) introduced the ratio of the dissipated strain energy to the total energy in analysing the rocking response of an anchored block. The strain energy in the  $P_0/W=0$  case before the fracture of the PT tendon is

$$SE = \frac{1}{2} F_u u_t \quad (11)$$

The kinetic energy of a SCW is considered to be zero at the verge of overturning ( $\theta=\alpha$ ). The potential energy (excluding the energy dissipation by viscous dampers and impacting) is given by

$$PE = mgR(1 - \cos \alpha) \approx mgR \frac{\alpha^2}{2} \quad (12)$$

The ratio of the dissipated energy to the total energy of a SCW is

$$\frac{SE}{PE} = \frac{F_u u_t}{mgR \alpha^2} \quad (13)$$

where  $u_t = F_u/k_p$  denotes the total elongation of the PT tendon

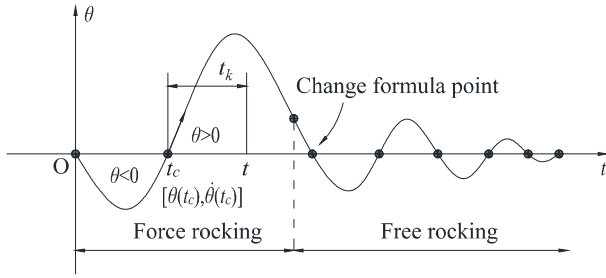


Fig. 4 Schematic diagram of the formula transformation

and it can also be approximated by  $\theta \cdot b$ .

The strain energy lost from the failure of the strands is approximately 51% of the energy that is needed to topple the free-standing wall. This value is much larger than the results for bridge piers given by Makris (0.6%), which are calculated based on the premise that  $F_u$  equals  $mg$ . These large differences indicate that the failure of PT strands easily induces the topple of the SCW. Therefore, the yielding of PT strands should be avoided in the design of SCWs.

#### 4 Linear analytical solution

Eq. (3) and its compact form shown by Eqs. (4) and (5) are applicable for arbitrary values of the rocking angle. For slender walls with small slenderness  $\alpha$ , the toppling usually happens at a low rocking angle and therefore Eq. (3) can be linearized. The trigonometric function of  $\theta$  can approximately be solved in order to avoid calculation difficulties. The linearization allows for the calculation of closed-form solutions when the seismic excitation is simplified a trigonometric form. Accordingly, the moment from the damper  $M_d$  is  $c\dot{\theta}(2b)^2$  and the moment  $M_t$  from the tendon is  $P_0b + k_p b^2 \theta$ , and Eq. (3) is reduced to

$$\begin{cases} I_o \ddot{\theta} + mgR(\alpha - \theta) + 4cb^2 \dot{\theta} + P_0b + k_p b^2 \theta + m\ddot{u}_g R = 0 & \theta > 0 \\ I_o \ddot{\theta} + mgR(-\alpha - \theta) + 4cb^2 \dot{\theta} - P_0b + k_p b^2 \theta + m\ddot{u}_g R = 0 & \theta < 0 \end{cases} \quad (14)$$

where  $f_1 = 6b^2 / R^2$ ,  $f_2 = (k_p b^2 - mgR) / mgR$ ,  $f_3 = (mgRa + P_0b) / mgR$ . Eq. (14) can be compacted with

$$\begin{cases} \ddot{\theta} + f_1 \zeta p \dot{\theta} + f_2 p^2 \theta = -\frac{\ddot{u}_g}{g} p^2 - f_3 p^2 \cdot \text{sgn}(\theta) & |\theta| \leq \theta_y \\ \ddot{\theta} + f_1 \zeta p \dot{\theta} - p^2 \theta = -\frac{\ddot{u}_g}{g} p^2 - p^2 \alpha \cdot \text{sgn}(\theta) & |\theta| > \theta_y \end{cases} \quad (15)$$

Accordingly, the solution of Eq. (15) should be presented for two segments  $|\theta| \leq \theta_y$  and  $|\theta| > \theta_y$ . Eq. (15) is a typical pattern of a nonhomogeneous equation with constant coefficients. The result  $\theta(t)$  should contain two vibration components: forced vibration and free vibration. It is assumed that the initial stiffness of the PT tendon is sufficiently large to keep  $k_p > mgR/b^2$ . Hence,  $f_2 > 0$  is reasonable for a SCW. SCWs are considered to be an underdamping system (Chopra 1995), and the damping for

the system satisfies the equation as follows

$$\zeta < \frac{2\sqrt{f_2}}{f_1} \quad (16)$$

The linear analytical solution can be expressed by Eq. (17) for the segment  $|\theta| \leq \theta_y$ ,

$$\theta(t) = e^{-\frac{\zeta p f_1}{2} t} [A_1 \cos(P_D t) + B_1 \sin(P_D t)] + C_1 \sin(\omega_g t + \varphi) + D_1 \cos(\omega_g t + \varphi) - \frac{f_3}{f_2} \text{sgn}(\theta) \quad (17)$$

where  $P_D = p\sqrt{4f_2 - f_1^2 \zeta^2} / 2$ . The equation for the angular velocities is directly obtained from the time derivatives of Eq. (17):

$$\begin{aligned} \dot{\theta}(t) &= -\frac{\zeta p f_1}{2} e^{-\frac{\zeta p f_1}{2} t} [A_1 \cos(P_D t) + B_1 \sin(P_D t)] + e^{-\frac{\zeta p f_1}{2} t} P_D [-A_1 \sin(P_D t) + B_1 \cos(P_D t)] \\ &\quad + \omega_g C_1 \cos(\omega_g t + \varphi) - \omega_g D_1 \sin(\omega_g t + \varphi) \\ C_1 &= \frac{a_g}{g} \frac{(\omega_g / p)^2 - f_2}{((\omega_g / p)^2 - f_2)^2 + f_1^2 \zeta^2 (\omega_g / p)^2} \\ D_1 &= \frac{a_g}{g} \frac{f_1 \zeta (\omega_g / p)}{((\omega_g / p)^2 - f_2)^2 + f_1^2 \zeta^2 (\omega_g / p)^2} \end{aligned} \quad (18)$$

where  $t_k = t - t_c$ . The constants  $A_1$  and  $B_1$  can be determined in terms of the initial rotation  $\theta(t_c)$  and initial angular velocity  $\dot{\theta}(t_c)$  in each phase and given by

$$\begin{aligned} A_1 &= \theta(t_c) - C_1 \sin(\omega_g t_c + \varphi) - D_1 \cos(\omega_g t_c + \varphi) + \frac{f_3}{f_2} \text{sgn}(\theta) \\ B_1 &= \frac{\dot{\theta}(t_c) - \omega_g C_1 \cos(\omega_g t_c + \varphi) + \omega_g D_1 \sin(\omega_g t_c + \varphi) + \zeta p f_1 A_1 / 2}{P_D} \end{aligned} \quad (19)$$

For the other segment  $|\theta| > \theta_y$ , Eq. (15) becomes

$$\theta = e^{-\frac{\zeta p f_1}{2} t} [A_2 \cosh(P_B t) + B_2 \sinh(P_B t)] + C_2 \sin(\omega_g t + \varphi) + D_2 \cos(\omega_g t + \varphi) + \alpha \text{sgn}(\theta) \quad (20)$$

where  $P_B = p\sqrt{4 + f_1^2 \zeta^2} / 2$ . The equations for the angular velocity are given by

$$\begin{aligned} \dot{\theta} &= -\frac{\zeta p f_1}{2} e^{-\frac{\zeta p f_1}{2} t} [A_2 \cosh(P_B t) + B_2 \sinh(P_B t)] + e^{-\frac{\zeta p f_1}{2} t} P_B [A_2 \sinh(P_B t) + B_2 \cosh(P_B t)] \\ &\quad + \omega_g C_2 \cos(\omega_g t + \varphi) - \omega_g D_2 \sin(\omega_g t + \varphi) \\ C_2 &= \frac{a_g}{g} \frac{1 + (\omega_g / p)^2}{((1 + (\omega_g / p)^2)^2 + f_1^2 \zeta^2 (\omega_g / p)^2)} \\ D_2 &= \frac{a_g}{g} \frac{f_1 \zeta (\omega_g / p)}{(1 + (\omega_g / p)^2)^2 + f_1^2 \zeta^2 (\omega_g / p)^2} \end{aligned} \quad (21)$$

$\theta(t_c)$  and  $\dot{\theta}(t_c)$  are assumed to be the angle of rotation and angular velocity in each initial phase, and then the constants  $A_2$  and  $B_2$  are:

$$\begin{aligned} A_2 &= \theta(t_c) - C_2 \sin(\omega_g t_c + \varphi) - D_2 \cos(\omega_g t_c + \varphi) - \alpha \text{sgn}(\theta) \\ B_2 &= \frac{\dot{\theta}(t_c) - \omega_g C_2 \cos(\omega_g t_c + \varphi) + \omega_g D_2 \sin(\omega_g t_c + \varphi) + \zeta p f_1 A_2 / 2}{P_B} \end{aligned} \quad (22)$$

Eqs. (17) and (18) and Eqs. (20) and (21) can be put together to build the time history of the rocking response of the SCW in the  $|\theta| \leq \theta_y$  case and  $|\theta| > \theta_y$  case, respectively. Fig. 4 shows the formula transformation in each phase.  $\text{sgn}(\theta) = -1$  is used in Eqs. (17) and (18) for  $\theta < 0$  when the time  $t$  is prior to  $t_c$ . At a specific time, the angle of rotation for a SCW changes from  $\theta < 0$  to  $\theta > 0$ , and the

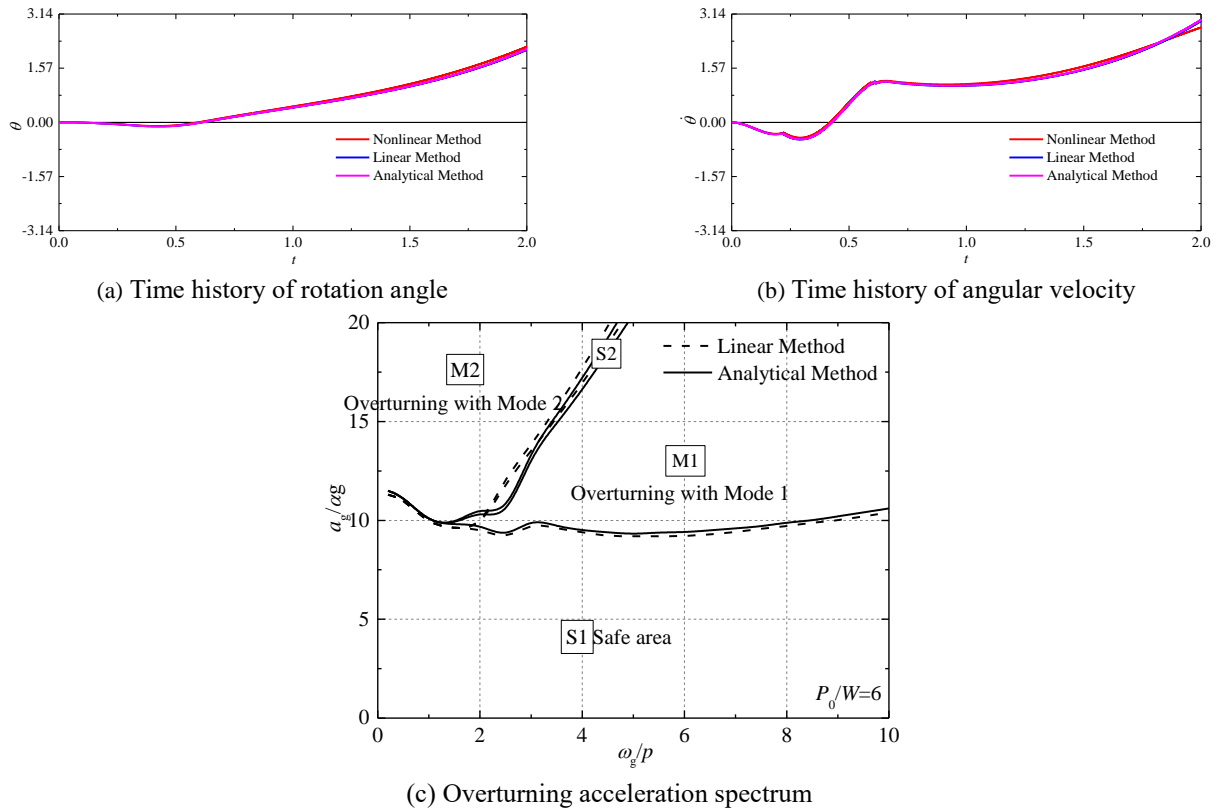


Fig. 5 Comparison of different solutions for a SCW

angular velocity  $\dot{\theta}$  should decrease on the basis of Eq. (7). New boundary conditions  $\theta(t_c)$  and  $\dot{\theta}(t_c)$  should be recorded as new initial conditions in the new rocking phase. Eq. (17) and Eq. (18) are used to compute the rocking response once again with  $t_k=t-t_c$  but with  $\text{sgn}(\theta)=1$  in this new phase. Note that the formula transformation repeats not only at the change of rotation angle  $\theta$  but also at the moment of the transition from force rocking to free rocking.

The linear analytical solution given by the foregoing equations will be validated using the numerical method with nonlinear and linear equations. Fig. 5 shows the results for a SCW for the case  $P_0/W=6$  under the one-sine pulse with the acceleration amplitude  $a_g=25 \text{ m/s}^2$  and the excitation frequency  $\omega_g=5p$ . All three solutions in Figs. 5(a)-(b) show a similar overturning process of a SCW with the fracture of the PT tendon. Three boundary lines with a median difference of -1.96%, 1.61% and 2.00% are respectively observed between the overturning plots of the linear method and analytical method. These numbers indicate a good agreement of the two solutions. The rocking responses calculated by the analytical method match well with the linear numerical method during the whole rocking process, which achieves a good approximation of the nonlinear numerical method. However, the differences are enlarged gradually over time compared to the nonlinear method, and this is mainly attributed to two reasons. One is the deviation accumulation of solving the differential equation and the initial condition. The other is that the linear approximation in Eq. (15) is based on the assumption of a small rotation and that the angle of rotation will increase with time. Fig. 5(c) gives the overturning acceleration spectrum for a SCW

using the linear solution with the analytical method and numerical method, displaying the good agreement of the two solutions. The linear solution also suggests that the minimum acceleration for a SCW overturning with Mode 1 exhibits little relationship with the excitation frequency.

## 5 Effect of the dampers coefficient

The energy dissipation capacity of a SCW is highly dependent on the viscous damper parameters except for the kinetic energy loss during each impact. To investigate the effects of the viscous damper, Four additional cases are developed using the structural details in the  $P_0/W=6$  case (see Fig. 3(d)), but with different values of damping coefficients ( $\zeta=3.45$ ;  $\zeta=5.75$ ;  $\zeta=8.05$  and  $\zeta=10.35$ ). The damping of the viscous damper is increased to investigate the effects of their enhanced performance on the boundary lines of the overturning plot, as shown in Fig. 6. This represents a reasonable range for the studied example because it clearly captures the process of the boundary change. Compared to the baseline case, the overturning region M2 exhibits gradual reduction and the overturning region M1 obviously shrinks and eventually closes in this range. These variations cause the area of the safe regions S1 and S2 increase with the increasing damping. The increasing damper force associated with a larger damping provides an enhanced lateral resistance in the rocking moment equilibrium since the failure of the strands happens when the acceleration amplitude is increased to create overturning of the wall.

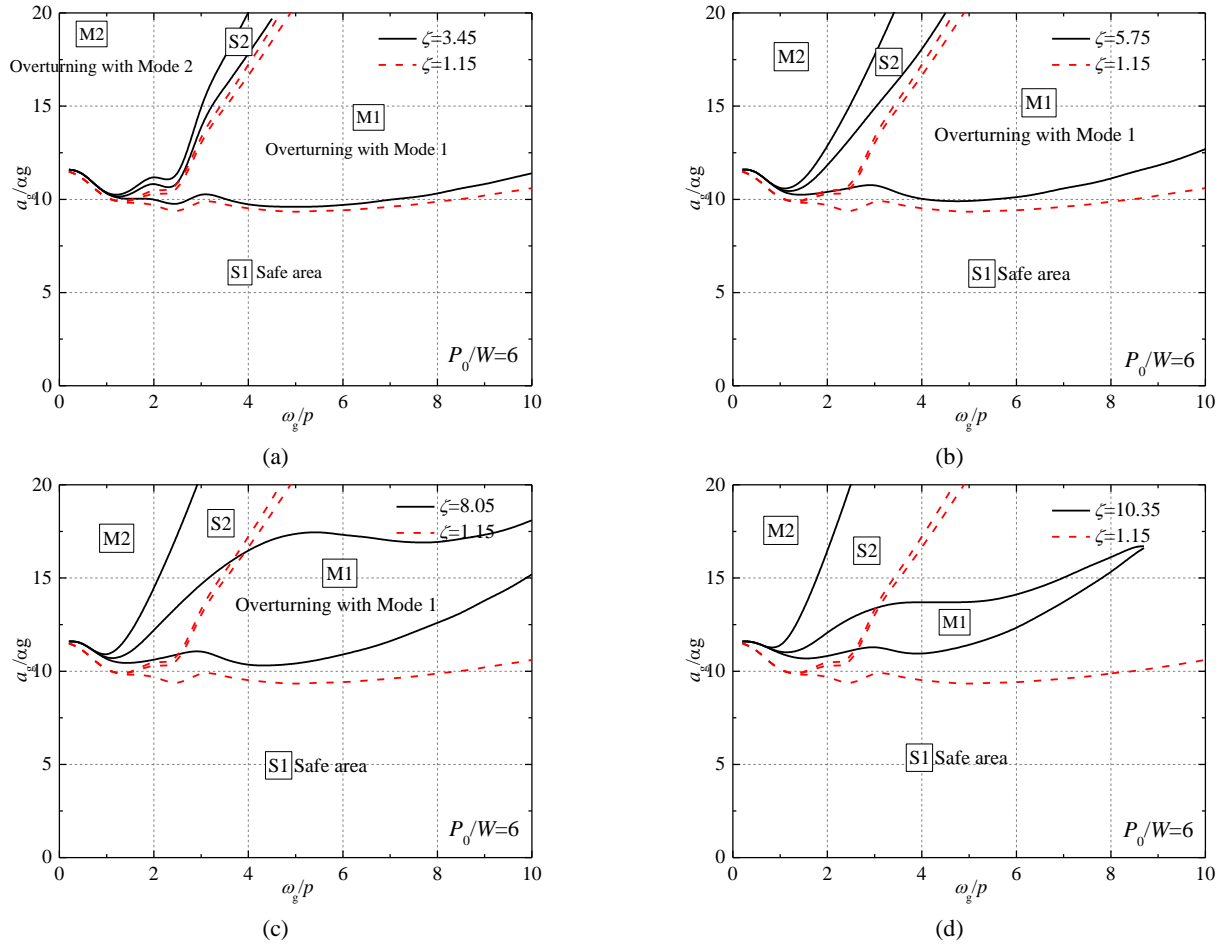


Fig. 6 Overturning influenced by viscous dampers with (a)  $\zeta=3.45$ ; (b)  $\zeta=5.75$ ; (c)  $\zeta=8.05$ ; (d)  $\zeta=10.35$

**6 Effect of the ductile behaviour of the PT tendon**

Seven-wire steel strands are the most common type of PT tendons used in SCW systems and are usually designed to be elastic during the designed earthquake events. Nevertheless, tendons may experience inelastic behaviour due to unexpected larger drift demands under extreme earthquakes. Although the aforementioned elastic-brittle model can simply represent this fracture behaviour of PT tendons, it cannot describe the ability of PT tendons to undergo large inelastic elongation prior to the fracture. The influence of the ductile behaviour of PT tendons on the collapse diagram of SCW is unclear. Fig. 7 shows a simplified bilinear model for PT tendons considering tension only. The Bouc-Wen hysteretic model has been adopted to describe the elastic-plastic behaviour of PT tendons, but it cannot capture the tension-only behaviour. A mathematical model of PT tendons is built to consider the elastic-plastic tension-only behaviour and is used to analyse the effects of the tendon plastic behaviour on the rocking of the SCW. This local subroutine is implemented in the computational modelling of the SCW to calculate the deformation and force of the tendon based on the geometric information from the rocking wall. It will shed some light on further studies to rebuild this material and investigate the nonlinear tendon behaviour of the tendon.

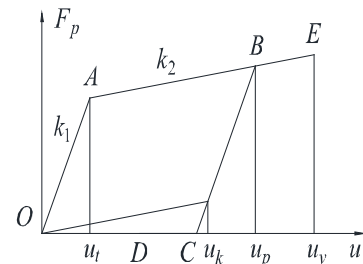


Fig. 7 Elastic-plastic behavior for PT tendon considering tension only

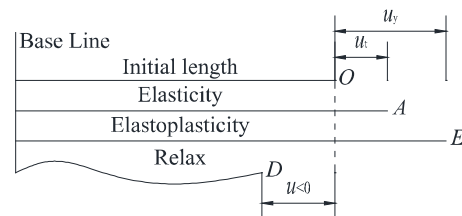


Fig. 8 State model for PT tendon

Fig. 8 shows the state model for PT tendons considering tension only. PT tendons remain elastic at the branch O→A.

$$F_p = k_1 u \tag{23}$$

where  $F_p$  denotes the inner force in the PT tendon,  $k_1$  denotes the elastic coefficient of the PT tendon, and  $u$  is the

corresponding deformation of the PT tendon.

The plastic strain of the PT tendon will take place at the branch A→B, and the force-displacement equation is:

$$F_p = k_1 u_y + k_2 (u - u_y) = k_2 u + (k_1 - k_2) u_y \quad (24)$$

where  $k_2$  denotes the yield coefficient of the PT tendon and  $u_y$  is the yield deformation of the PT tendon.

During the unloading from the branch B→C, the equation of the PT tendon can be expressed as

$$F_p = k_1 u - (k_1 - k_2)(u_p - u_y) \quad (25)$$

where  $u_p$  denotes the x-coordinate of the unloading point at the branch A→B.

The inner force  $F_p$  decreases to 0 when the PT tendon relaxes:

$$F_p = 0 \quad (26)$$

The reloading path is D→C→B→E until the PT tendon ruptures.

To exactly describe the inelastic behaviour of the PT tendon, an auxiliary line passing through the zero point and parallel to the branch A→B is constructed to intersect the branch B→C. The x-coordinate of the intersection point is  $u_k$ .  $s$  denotes the status of the PT tendon ( $s=0$  for the line OA and BC;  $s=1$  for the line AB and  $s=-1$  for the line CO). Therefore, there are three states for this tendon material, State 1 ( $s=0$ ), State 2 ( $s=1$ ) and State 3 ( $s=-1$ ). The compact form of Eqs. (23) - (26) is given by

$$F_p = k u + R_p \quad (27)$$

State 1 represents the tendon being loaded with the input of  $k=k_1$  and  $R_p=-(k_1-k_2)u_k$ , State 2 represents the branch with the input of  $k=k_2$  and  $R_p=(k_1-k_2)u_t$  and State 3 represents the load path with the input of  $k=0$  and  $R_p=0$ . The transitions of the three states are presented in the Eqs. (28) - (30). When the condition of the state change is satisfied, the value of the indicator  $s$  will be changed, and the material behaviour in the new state is used in the analysis.

$$s = 0 \Rightarrow \left\{ \begin{array}{l} k = k_1, R_p = -(k_1 - k_2)u_k \\ u - u_k \geq u_t \ \& \ \dot{u} > 0 \rightarrow s = 1 \\ u < u_k - k_2 u_k / k_1 \ \& \ \dot{u} \leq 0 \rightarrow s = -1 \end{array} \right\} \quad (28)$$

$$s = 1 \Rightarrow \left\{ \begin{array}{l} \dot{u} > 0 \rightarrow k = k_2, R_p = (k_1 - k_2)u_t \\ \dot{u} < 0 \rightarrow s = 0, u_k = u_p - u_t \end{array} \right\} \quad (29)$$

$$s = -1 \Rightarrow \left\{ \begin{array}{l} \dot{u} \leq 0 \rightarrow k = 0, R_p = 0 \\ \dot{u} > 0 \ \& \ u > u_k - k_2 u_k / k_1 \rightarrow s = 0 \end{array} \right\} \quad (30)$$

The equation between the angle of rotation  $\theta$  and the displacement at the end of the PT tendon  $\mu$  is given by

$$u \approx P_0 / k_1 + 2b \left| \sin\left(\frac{\theta}{2}\right) \right| \quad (31)$$

Conditional statements ( $\mu > \mu_y$ ) are used to determine whether the yielding of the strands are being reached. The yielding deformation of the tendon  $\mu_y$  can be calculated using the stress at yield and the modulus of elasticity reported in previous experiments (Bruce and Eatherton 2016). The program will evaluate if the tendon deformation  $\mu$ , including the initial PT deformation ( $P_0/k_1$ ) and the superimposed deformation due to loading ( $2b|\sin(\theta/2)|$ ), is larger than the yielding strain at each increment. Once the *if* condition is met, State 2 ( $s=1$ ) will be executed.

After substitution of Eq. (27) into Eq. (4), it holds,

$$\underbrace{[I_s \ddot{\theta} + mgR \sin(\alpha \cdot \text{sgn}(\theta) - \theta)]}_{\text{rocking wall}} + \underbrace{c \dot{\theta} \cdot (2b \cos \frac{\theta}{2})^2}_{\text{damper}} + \underbrace{F_p \cdot (b \cos \frac{\theta}{2}) \cdot \text{sgn}(\theta)}_{\text{tendon}} = \underbrace{-m \ddot{u}_t R \cos(\alpha \cdot \text{sgn}(\theta) - \theta)}_{\text{seismic excitation}} \quad (32)$$

To verify the formula describing the elastic-plastic behaviour of the PT tendon, an example of a PT tendon with an effective length  $l=5$  m and the initial PT force  $P_0=0$  kN is used. The parameters for the elastic-plastic behavior of the PT tendon are chosen based on the previous experiments (Bruce and Eatherton 2016). The mean experimental results of the testing series BD/SU are input for the backbone curve of the tendon material. The yield strength defined as the force at 1% elongation is 1728 MPa and the peak strength is 1918 MPa. The load carrying capacity of the seven-wire strand experiences a sudden loss at every fracture of individual wires. The initial wire fracture is a limit state that should be avoided in a specified design level and therefore the deformation capacity of the seven-wire strand prior to initial wire fracture was recorded for different testing series. The strain at first wire fracture 3.3% is chosen as the fracture limit. Once this strain limit is reached, the tendon is removed immediately from the model. The tested tendon at one end is fixed, and the enforced sinusoidal type displacement is applied to the tendon at the other end. A sinusoidal type displacement function with a maximum displacement of 0.165 m and a cosinoidal-type velocity function are used and the respective expressions are given by

$$u = 0.165 \sin(2\pi t) \quad (33)$$

$$\dot{u} = 0.165 \times 2\pi \cos(2\pi t) \quad (34)$$

Fig. 9 shows the stiffness coefficient and the force-displacement of the PT tendon. Peak A in Fig. 9(a) is the status where the PT tendon enters the plastic status instantly after reloading to maximum displacement and before unloading again. Fig. 9(b) shows the force-displacement curve of the tested PT tendon. The force in the tendon becomes zero after the tendon enters into the compression state. These results suggest that the given model can clearly describe the elastic-plastic tension-only behaviour of the PT tendon

The overturning acceleration spectrum computed by Eq. (32) is shown in Fig. 10, along with the results from a SCW considering the elastic-brittle PT tendon. It demonstrates that a SCW with the elastic-plastic tendon also has two overturning modes. Extra excitation energy will be dissipated after the PT tendon sustains plastic deformation, resulting in high levels of acceleration required for a SCW

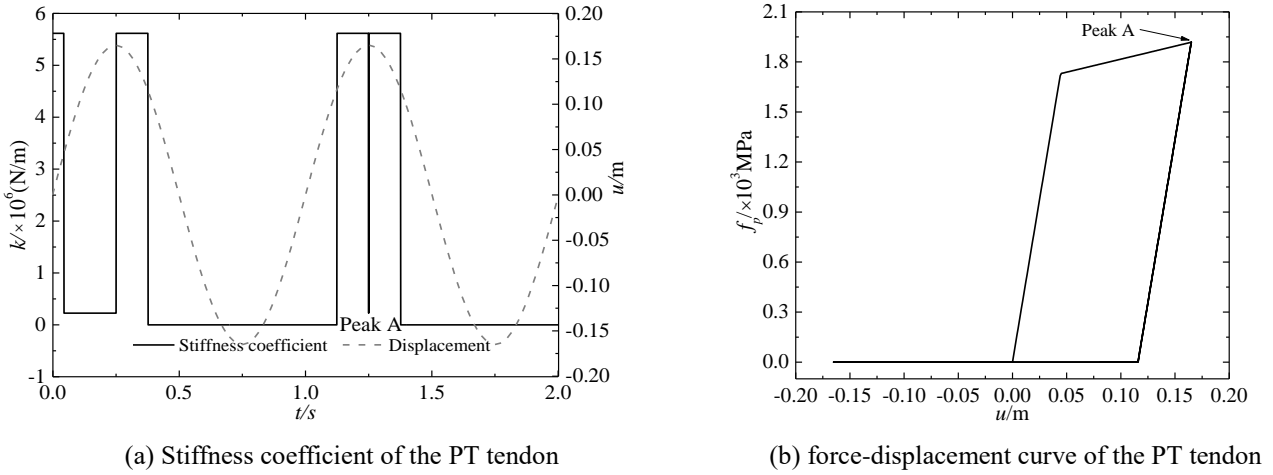


Fig. 9 State model for PT tendons

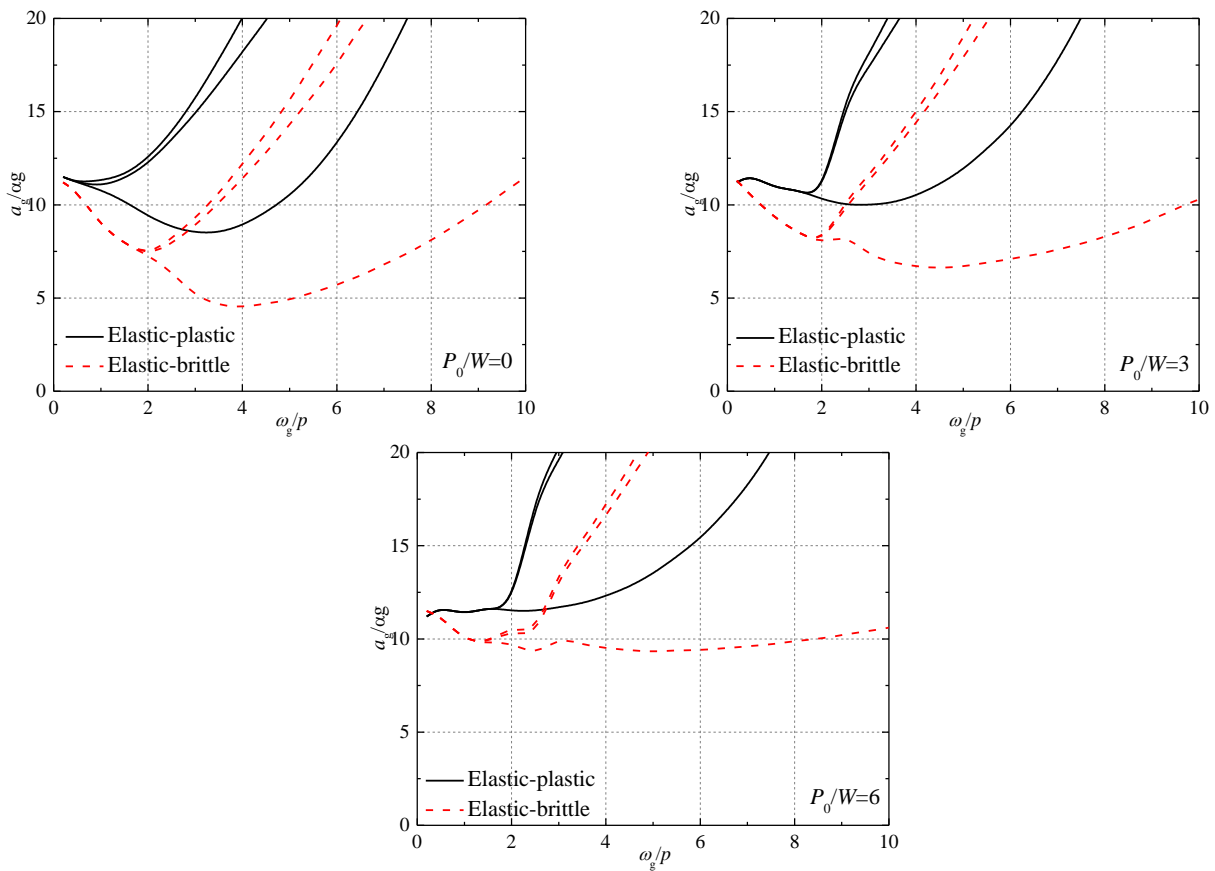


Fig. 10 Overturning acceleration spectrum with different fracture displacement ratios

to rock in the elastic-plastic case. It can be observed in Fig. 10 that the minimum overturning acceleration is increased significantly in the whole range of the studied  $w_g/p$  after the plastic elongation of the tendon is considered. For large values of  $w_g/p$ , the increase of the PT force has a limited influence on the upper limit of the safe region S1, indicating that the enhanced stability of the wall is found to be relatively independent of the initial PT force when the wall size or the pulse frequency is increased. For small values of  $w_g/p$ , the upper limit of the safe region S1 tends to be a horizontal line with increasing initial force. The safe region

S2 shifts upward and shrinks with the increase of the PT force. These results are consistent with those of a SCW using an elastic-brittle PT tendon.

### Conclusions

This paper investigated the rocking responses of self-centering walls (SCWs) with base viscous dampers under a sinusoidal type pulse. The inelastic behaviour of the tendon is considered. The main conclusions of the study are as

follows:

- SCWs with viscous dampers have similar rocking states to free-standing walls under a sinusoidal type pulse. Higher acceleration is needed to topple a SCW in response to a low-frequency pulse after the implementation of a PT tendon and viscous dampers. The overturning region with Mode 1 in the PT force cases separates the safe region of the wall into two parts: the region S1 with an elastic tendon and S2 with a fractured tendon. The minimum overturning acceleration of a SCW with an elastic-brittle tendon becomes insensitive to excitation frequency as the PT force increases.
- The exact analytical solution to the linear approximate equation of motion is provided for a slender SCW. The rocking responses calculated by the linear analytical solution match well with the linear numerical solution during the whole rocking process and achieve a good approximation of the nonlinear numerical solution.
- A simplified bilinear model for a PT tendon is constructed to describe the elastic-plastic behaviour of PT tendons. Two overturning types still exist in the wall when considering the elastic-plastic behaviour of the PT tendon. The minimum overturning acceleration is increased significantly in the whole range of the studied  $w_g/p$  after the plastic elongation of the tendon is considered.

## Acknowledgements

The research described in this paper was sponsored by \ "National Key R&D Program of China" (2018YFC0705), \ "The Fundamental Research Funds for the Central Universities" (2242019K40083) and \ "Scientific Research Fund of Institute of Engineering Mechanics, China Earthquake Administration" (2019EEEEVL0303). The supports are gratefully acknowledged.

## References

- Alavi, B. and Krawinkler, H. (2004), "Behavior of moment - resisting frame structures subjected to near - fault ground motions", *Earthq. Eng. Struct. Dyn.*, **33**(6), 687-706. <https://doi.org/10.1002/eqe.369>.
- Aaleti, S. and Sritharan, S. (2009), "A simplified analysis method for characterizing unbonded post-tensioned precast wall systems", *Eng. Struct.*, **31**(12), 2966-2975. <https://doi.org/10.1016/j.engstruct.2009.07.024>.
- Apostolou, M., Gazetas, G. and Garini, E. (2007), "Seismic response of slender rigid structures with foundation uplifting", *Soil Dyn. Earthq. Eng.*, **27**(7), 642-654. <https://doi.org/10.1016/j.soildyn.2006.12.002>.
- Bray, J.D. and Rodriguez-Marek, A. (2004), "Characterization of forward-directivity ground motions in the near-fault region", *Soil Dyn. Earthq. Eng.*, **24**(11), 815-828. <https://doi.org/10.1016/j.soildyn.2004.05.001>.
- Bruce, T.L. and Eatherton, M.R. (2016), "Behavior of post-tensioning strand systems subjected to inelastic cyclic loading", *J. Struct. Eng.*, **142**(10), 04016067. [https://doi.org/10.1061/\(ASCE\)ST.1943-541X.0001503](https://doi.org/10.1061/(ASCE)ST.1943-541X.0001503).
- Chopra, A.K. (1995), *Dynamics of Structures*, Prentice-Hall: Englewood Cliffs, N.J.
- Dimitrakopoulos, E.G. and Giouvanidis, A.I. (2015), "Seismic response analysis of the planar rocking frame", *J. Eng. Mech.*, **141**(7), 04015003. [https://doi.org/10.1061/\(ASCE\)EM.1943-7889.0000939](https://doi.org/10.1061/(ASCE)EM.1943-7889.0000939).
- Dimitrakopoulos, E.G. and DeJong, M.J. (2012), "Overturning of retrofitted rocking structures under pulse-type excitations", *J. Eng. Mech.*, **138**(8), 963-972. [https://doi.org/10.1061/\(ASCE\)EM.1943-7889.0000410](https://doi.org/10.1061/(ASCE)EM.1943-7889.0000410).
- ElGawady, M.A., Ma, Q., Butterworth, J.W. and Ingham, J. (2011), "Effects of interface material on the performance of free rocking blocks", *Earthq. Eng. Struct. Dyn.*, **40**(4), 375-392. <https://doi.org/10.1002/eqe.1025>.
- Eom, T., Kang, S. and Kim, O. (2014), "Earthquake resistance of structural walls confined by conventional tie hoops and steel fiber reinforced concrete", *Earthq. Struct.*, **7**(5), 843-859. <https://doi.org/10.12989/eas.2014.7.5.843>.
- Feng, R., Chen, Y. and Cui, G. (2018), "Dynamic response of post-tensioned rocking wall-moment frames under near-fault ground excitation", *Earthq. Struct.*, **15**(3), 243-251. <https://doi.org/10.12989/eas.2018.15.3.243>.
- Giouvanidis, A.I. and Dimitrakopoulos, E.G. (2017), "Seismic performance of rocking frames with flag-shaped hysteretic behavior", *J. Eng. Mech.*, **143**(5), 04017008. [https://doi.org/10.1061/\(ASCE\)EM.1943-7889.0001206](https://doi.org/10.1061/(ASCE)EM.1943-7889.0001206).
- Housner, G.W. (1963), "The behavior of inverted pendulum structures during earthquakes", *Bull. Seismol. Soc. Amer.*, **53**(2), 403-417.
- Kurama, Y.C., Sause, R., Pessiki, S. and Lu, L.W. (2002), "Seismic response evaluation of unbonded post-tensioned precast walls", *ACI Struct. J.*, **99**(5), 641-651.
- Lim, W.Y. and Hong, S.G. (2014), "Cyclic loading tests for precast concrete cantilever walls with C-type connections", *Earthq. Struct.*, **7**(5), 753-777. <https://doi.org/10.12989/eas.2014.7.5.753>.
- Makris, N. and Vassiliou, M.F. (2014), "Dynamics of the rocking frame with vertical restrainers", *J. Struct. Eng.*, **141**(10), 04014245. [https://doi.org/10.1061/\(ASCE\)ST.1943-541X.0001231](https://doi.org/10.1061/(ASCE)ST.1943-541X.0001231).
- Makris, N. and Roussos, Y.S. (2000), "Rocking response of rigid blocks under near-source ground motions", *Geotechnique*, **50**(3), 243-262. <https://doi.org/10.1680/geot.2000.50.3.243>.
- Makris, N. and Zhang, J. (2001), "Rocking response of anchored blocks under pulse-type motions", *J. Eng. Mech.*, **127**(5), 484-493.
- Mavroeidis, G.P. and Papageorgiou, A.S. (2003), "A mathematical representation of near-fault ground motions", *Bull. Seismol. Soc. Amer.*, **93**(3), 1099-1131. <https://doi.org/10.1785/0120020100>.
- Palermo, D., Vecchio, F.J. and Solanki, H. (2002), "Behavior of three-dimensional reinforced concrete shear walls", *ACI Struct. J.*, **99**(1), 81-89.
- Perez, F.J., Pessiki, S. and Sause, R. (2004), "Seismic design of unbonded post-tensioned precast concrete walls with vertical joint connectors", *PCI J.*, **49**(1), 58-79.
- Perez, F.J., Pessiki, S. and Sause, R. (2013), "Experimental lateral load response of unbonded post-tensioned precast concrete walls", *ACI Struct. J.*, **110**(6), 1045-1055.
- Perez, F.J., Sause, R. and Pessiki, S. (2007), "Analytical and experimental lateral load behavior of unbonded posttensioned precast concrete walls", *J. Struct. Eng.*, **133**(11), 1531-1540. [https://doi.org/10.1061/\(ASCE\)0733-9445\(2007\)133:11\(1531\)](https://doi.org/10.1061/(ASCE)0733-9445(2007)133:11(1531)).
- Restrepo, J.I. and Rahman, A. (2007), "Seismic performance of self-centering structural walls incorporating energy dissipators", *J. Struct. Eng.*, **133**(11), 1560-1570. [https://doi.org/10.1061/\(ASCE\)0733-9445\(2007\)133:11\(1560\)](https://doi.org/10.1061/(ASCE)0733-9445(2007)133:11(1560)).
- Sritharan, S., Beyer, K., Henry, R.S., Chai, Y.H., Kowalsky, M.

- and Bull, D. (2014), "Understanding poor seismic performance of concrete walls and design implications", *Earthq. Spectra*, **30**(1), 307-334.
- Vassiliou, M.F. and Makris, N. (2015), "Dynamics of the vertically restrained rocking column", *J. Eng. Mech.*, **141**(12), 04015049. [https://doi.org/10.1061/\(ASCE\)EM.1943-7889.0000953](https://doi.org/10.1061/(ASCE)EM.1943-7889.0000953).
- Xu, L., Xiao, S. and Li, Z. (2018), "Hysteretic behavior and parametric studies of a self-centering RC wall with disc spring devices", *Soil Dyn. Earthq. Eng.*, **115**, 476-488. <https://doi.org/10.1016/j.soildyn.2018.09.017>.
- Zhang, J. and Makris, N. (2001), "Rocking response of free-standing blocks under cycloidal pulses", *J. Eng. Mech.*, **127**(5), 473-483. [https://doi.org/10.1061/\(ASCE\)0733-9399\(2001\)127:5\(473\)](https://doi.org/10.1061/(ASCE)0733-9399(2001)127:5(473)).